Geophys. J. Int. (2006) **167,** 1220–1232 doi: 10.1111/j.1365-246X.2006.03083.x

Pre-collapse identification of sinkholes in unconsolidated media at Dead Sea area by 'nanoseismic monitoring' (graphical jackknife location of weak sources by few, low-SNR records)

Gilles Hillel Wust-Bloch[1] and Manfred Joswig[2]

[1] *Department of Geophysics and Planetary Sciences, Tel Aviv University, Tel Aviv* 69978, *Israel*
[2] *Institut für Geophysik, Universität Stuttgart,* 70174 *Stuttgart, Germany. E-mail: joswig@geophys.uni-stuttgart.de*

Accepted 2006 May 19. Received 2006 May 15; in original form 2004 August 13

SUMMARY

The sudden failure of near-surface cavities and the resulting sinkholes have constituted a recent hazard affecting the populations, lifelines and the economy of the Dead Sea region. This paper describes how seismic monitoring techniques could detect the extremely low-energy signals produced by cavitation in unconsolidated, layered media. Dozens of such events were recorded within a radius of 200 m during several night-time experiments carried out along the western Dead Sea shores.

The absence of prior knowledge about cavitation-induced events in unconsolidated media required an initial signal characterization, for which a series of source processes were simulated in the field under controlled conditions. The waveform analysis by sonograms recognizes two main groups of seismic events: impacts on dry material and impacts in liquid. Our analysis demonstrates that the discrimination between both types of source functions is robust despite the extreme nature of the scatter media.

In addition to their association with specific source processes, these events can be precisely located by a graphical, error-resistant jackknifing approach. Using an extended M_L scale, their source energy can be quantified, and related to standard seismic activity. In summary, it is now possible to monitor subsurface material failures before sinkhole collapse since the discrimination of impact signals on the basis of their frequency content is indicative of the maturity of the cavitation process.

Key words: cavitation, Dead Sea area, jackknife location, sinkhole activity, sonograms.

INTRODUCTION

Cavitation and related subsurface material failures are dynamic processes that cannot be monitored by geophysical mapping methods providing one-time snapshots of the subsurface. Our aim is to complement the mapping by seismic monitoring that can continuously record subsurface material failures. Our success depends on a combination of matched, innovative techniques called 'nanoseismic monitoring' that differ significantly from standard microseismic or microearthquake networks (e.g. Lee & Stewart 1981). There one may process weak events too, but based on favourable site conditions, like borehole arrays or seismic networks in mines; recording close to source yields sufficient amplitudes for reliable phase picking. 'Nanoseismic monitoring' deals with the other extreme: resolution at the limits of noise level, ambiguous phase readings, and just a few available stations (Joswig 2005). This is our scenario of monitoring sinkhole collapse in regions up to one km^2 with limited equipment resources. The subsurface failures consist mainly of material impacts triggered by cavitation: short freefall (several metres) of a natural rock mass ranging in weight from a few to dozens of kilograms. Given the extremely low energy of the source processes with an equivalent M_L of -3.0 and below, the seismological challenge resides in detecting and distinguishing them in the most unfavourable signal-to-noise ratios (SNR). In addition, the inhomogeneous, layered and unconsolidated nature of the media is expected to cause high scattering of the waveforms, making phase onsets difficult to pick.

Other applications of 'nanoseismic monitoring' include landslides, rapid aftershock surveys, on-site inspections (OSI) of CTBTO for aftershocks from underground nuclear explosions, and mapping of active faults (Joswig 2005). Always the target of monitoring are seismic signals below M_L 0.0 which could by good reason be addressed as 'nanoearthquakes' (Butler 2003). The standard, night-time location performance of 'nanoseismic monitoring' achieved by surface-sited SNS in several, recent field campaigns was $M_L - 1.0$ in 10 km distance, or $M_L - 2.0$ in 3 km distance.

Sinkholes, the surface expression of cavitation, as well as associated subsurface material failure processes, have been observed to

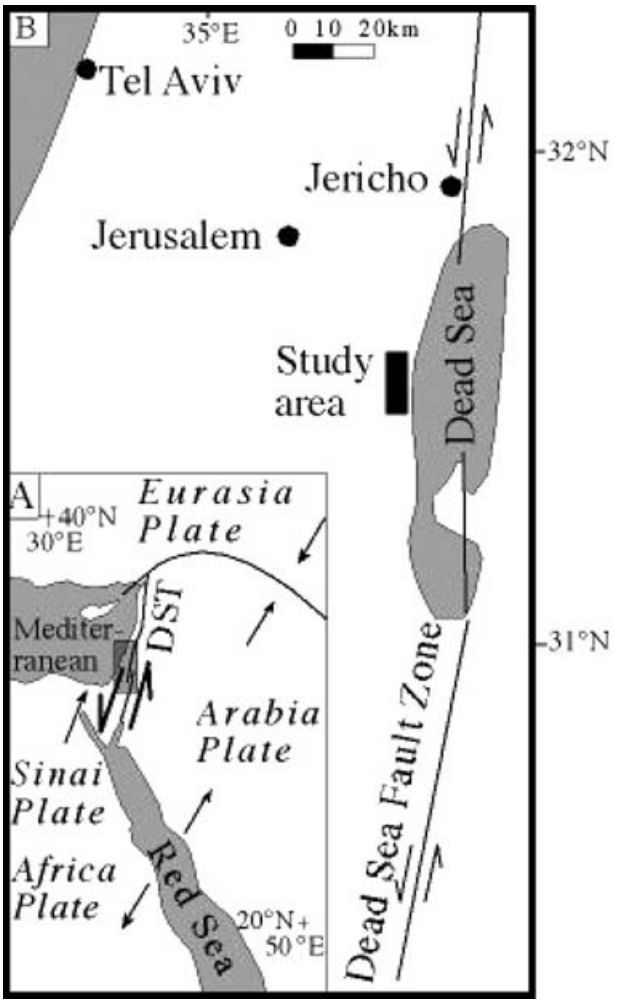

Figure 1. Maps of the Dead Sea area with global tectonic set-up (a) and the location of the study area (black rectangle) along the western Dead Sea shores (b).

stud the Israeli and Jordanian shores of the Dead Sea (Fig. 1) over the past two decades (Arkin & Gilat 1999; Taqieddin *et al.* 2000; Wachs *et al.* 2000; Abelson *et al.* 2003; Yechieli *et al.* 2004; Closson *et al.* 2005). The lowering of the Dead Sea level, at a rate of about 0.5 m yr^{-1}, over the past 40 yr is considered to be the main factor contributing to intense sinkhole development (Wachs *et al.* 2000). A dropping of the brine/salt-water groundwater level has put fresh groundwater from the mountain aquifers in direct contact with shallow 10 000-yr-old salt deposits along the seashores, thus initiating cavitation by salt dissolution. However, both the exact dynamics of groundwater and the cavitation process itself remains the subject of much debate (Arkin & Gilat 1999; Wachs *et al.* 2000).

Sinkhole hazard along the Dead Sea shores has triggered a wide range of investigations, from simple field observations and airborne mapping to sophisticated geophysical surveys. Individual sinkholes or clusters of sinkholes have been surveyed in detail over the past few years throughout the western Dead Sea shores (Itamar & Reizmann 2000; Raz 2000) and integrated in a GIS (Abelson *et al.* 2002). Geodetic monitoring of surface deformation, using InSAR and GPS observations (Schattner 2003) is the only quantitative modelling of sinkhole development available today. Schattner (2003) distinguished between two types of deformations processes: the local deformation directly associated to individual sinkholes and the more regional deformation related to the evolution of sinkhole clusters. Field observations and InSAR measurements of surface deformation show that several sinkhole areas are aligned along fault zones or delimit zones of local subsidence (Baer *et al.* 2002; Abelson *et al.* 2002; Yechieli *et al.* 2004). Because these bimodal features are subparallel to ENE trending fault zones (Abelson *et al.* 2003) it was suggested that sinkhole development is controlled by tectonics (Yechieli *et al.* 2004). However the tectonic control of sinkhole dynamics, via fresh groundwater, is far from ubiquitous. Several sinkhole clusters still develop randomly, controlled neither by fault zones, nor guided by fresh/salt water interface that gradually retreats towards the shoreline. No unequivocal relationship has yet been established to directly linking the cavitation processes at depth and sinkhole failure at surface. Several geophysical techniques that have been applied in sinkhole environments elsewhere (Wenjin & Jiajian 1990; Nelson & Haigh 1990), were also applied to detect cavities along the Dead Sea shores (Kafri *et al.* 1997; Rybakov *et al.* 2000; Shtivelman 1999; Wachs *et al.* 2000). Microgravimetry surveys show that anomalous mass deficit generally, but not unequivocally, coincides with zones of existing sinkholes (Rybakov *et al.* 2000), suggesting again that the complex features of subsurface cavities are beyond the resolution capabilities of the method. Even if the imaging resolution of these geophysical techniques were to improve drastically, monitoring cavitation dynamics remains beyond their scope.

Although no comprehensive model exists today for sinkhole development in the Dead Sea area, data from some of the aforementioned investigations were useful for constraining field parameters and for designing a schematic cavity model (Fig. 2). The model is based on borehole (Hever-2) and groundwater data that are available for the Nachal Hever area (Yechieli 2002) as well as from observation of material outcropping in the field. The subsurface (0–23 m) consists of a mixture of fine lake deposits (clay) and alluvial fan material (gravel) resting on a 5–6-m-thick solid salt unit (Yechieli 2002). The top sediments are composed of alternating layers of varying thickness (0.1–10 cm) with gravel, sand, silt and clay as well as millimetre-thick laminae of aragonite and salt (see photo of Fig. 2). Due to the complex interaction of high-energy flash-flood deposits of the Hever stream, the lateral material continuity is irregular and material variations can be extreme within a few metres. The bottom of the salt units at 35 m depth, which controls the maximal depth of cavity, is the only reliable constraint available. Though cavitation is initially confined to the salt unit, the composite nature of the overlying sediments results in the development of cavities and material discontinuities that can have widely varying shapes and sizes. Cavities can be either air-filled or brine-saturated, depending on the position of the groundwater level, which is stable (Yechieli, personal communication, 2005) around 20 m below the surface and nearly coincides with the top of the salt unit at Hever-2 (Yechieli 2002). The material that fails from the roof will impact either at the surface of the brine, or on dry loose debris material that previously collapsed from the roof of the cavity, dissipating part of the shock energy. Nanoseismic monitoring techniques will be used to verify, first, whether the tentative cavitation model of Fig. 2 that was designed on the basis of existing data generates low-energy signals and, second, whether these signals corroborate those produced by field simulations under controlled conditions.

DATA ACQUISITION AND PROCESSING

Following an initial survey of seismic ground noise at several sinkhole locations along the western Dead Sea shores (Joswig *et al.*

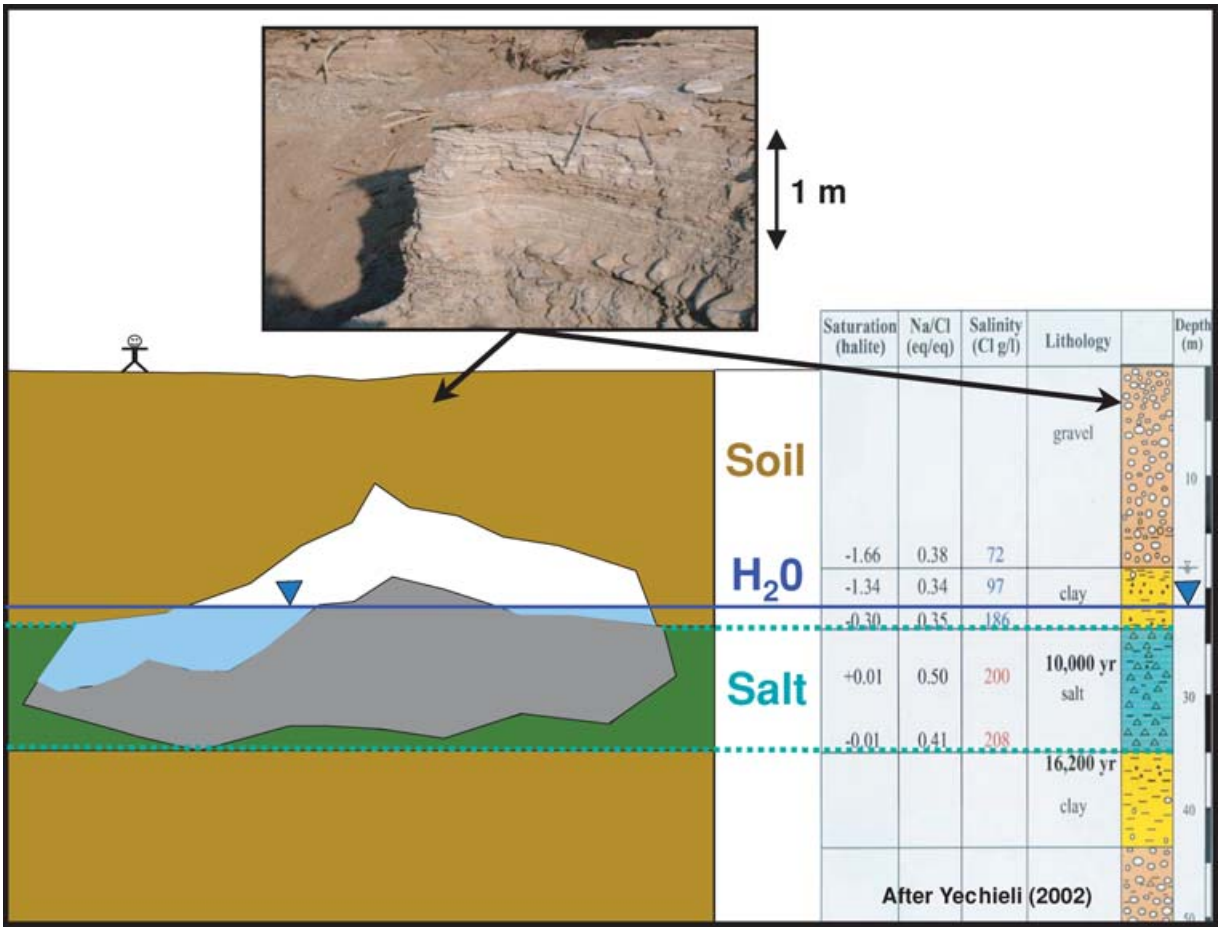

Figure 2. Schematic diagram of a sinkhole and mature cavity in the subsurface according to local borehole log (Yechieli 2002) with detailed photograph of the layered media. Groundwater depth is below 20 m and salt is found between 23 and 35 m depth.

2002), a study area (Fig. 1) located on the northern section of Nachal Hever (NH) alluvial fan was selected for a feasibility study. This site (see airphoto in background of Fig. 8), previously investigated for its sinkhole activity (Schattner 2003), is located 400 m south from the Dead Sea shore and over 1,500 m from the nearest known source of anthropogenic noise (National Road #90 and Ein Gedi SPA). Night-time peak-to-peak ground noise amplitudes of 180 nm s^{-1} for 0.3–10 Hz compare well with the stable ground noise level of 100 nm s^{-1} for 0.3–10 Hz recorded at the subsurface EIL station of the Israel Seismic Network (ISN)/International Monitoring System (IMS) of CTBTO, some 200 km south. Though more than 400 hr of continuous recording were acquired at different sinkhole sites along the Dead Sea shores, the present study focuses on four data sets of over 12 continuous hours each, recorded at night at the identical NH site (N 31° 41.380; E 35° 38.590). The data sets are HEV-1 (2002.02.13/14), HEV-2 (2002.05.02/03), HEV-3 (2003.01.20/21) and HEV-4 (2003.05.22/23) . SNR of HEV-1 and HEV-3 data sets, both accidentally recorded during rainstorms that brought traffic on national road #90 to a complete standstill, is better than that of HEV-2 and HEV-4. Prevalent vandalism in the area prevented monitoring over extended periods of time for this feasibility study.

Data was acquired and processed using the approach of 'nanoseismic monitoring' (Joswig 2005) based on Seismic Navigation Systems (SNS) and the SparseNet software suite. The six-channel SNS consists of four short-period sensors: One single three-component sensor at the centre of the configuration and three vertical component sensors at the periphery. 0–120–240° deployment geometry around the central sensor, together with a SNS aperture of 45 m (Fig. 9), provided optimal event coverage for most sinkhole clusters while providing near-plane wave conditions for events originating from neighbouring sinkhole clusters, 200–300 m away.

Sonograms (Fig. 3), which are broad-band, self-adaptive filters for temporary signal energy (Joswig 1995), were utilized to allow for semi-automated data processing. They are optimized by customized muting, pre-whitening and log-scaling schemes to display the f-t distribution of signal energy within a 0.1–75 Hz band. Sonogram-supported pattern recognition schemes (Joswig 1990) were initially applied to screen-out between dozens of large-amplitude signal types including regional and local earthquakes as well as common noise sources such as traffic, planes and pumping systems. In screening our sinkhole data, we could heuristically identify six different sonogram patterns of potential low-energy events (Fig. 3); however, their association with distinct source processes could only be validated after calibration experiments.

Two modules of the SparseNet software (Joswig 1999) were ran: SonoDet detected an average (on six traces) of 2000–2500 hits per period of 12 hr, which were then processed by MatchNet (ex Coassein). This rule-based system evaluates event coincidence on multi-trace records. The final voting list selects events (approximately 100 per 12 hr) that have been detected on two or more individual traces and provides a series of additional signal quality factors on the basis of which individual seismic events are located.

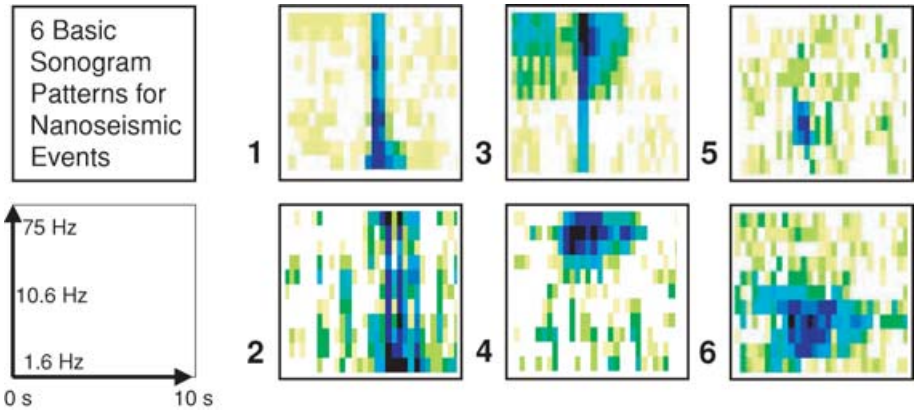

Figure 3. Classification of seismic signals by sonogram analysis. Heuristically, six basic signal patterns have been identified and sorted into three subgroups: spikes (#1 and #2), high-frequency events (#3 and #4) and low-frequency events (#5 and #6). For identification of source processes see text.

Finally, event analysis and location was carried out manually, using the new HypoLine module of SparseNet. This interactive, graphics-based evaluation program utilizes simultaneously network and array processing tools, spectral and polarization analysis, and displays uncertainty ranges of overdetermined systems for location and beam forming by jackknifing instead of residuals (Joswig 2005). The HypoLine screen dump in Fig. 4 shows an $M_L - 2.7$ event of the 2002 May data set located 74 m off the centre station, that is, outside the SNS aperture. The permutation of four P onsets by jackknifing gave six hyperbolae for the onset differences, complemented by one $t_S - t_P$ circle from the 3-C centre site (shown as double circle with uncertainty range), and eventual array beams (only determined for sufficient plane wave propagation). All lines intersect as function of layer model and depth constraint; the best epicentre approximation is found for the most focussed intersection layout. By this approach, HypoLine allows for the determination of origin time, epicentre, depth, suited half-space v_p and v_s, and M_L already by one single SNS (i.e. four seismometers). The example of Fig. 4 marks quite the limits of SNR in event processing; still slight improvements of half magnitude could be achieved by the dynamic features of HypoLine (not shown here) where parameter changes cause real-time updates of all location constraints.

In our sinkhole monitoring set-up, the lateral location accuracy is in the order of metres for events located in network mode (within twice the aperture of SNS); else array-mode event location yields lateral accuracy of $\pm 10^\circ$. Source location could be significantly optimized by deploying several SNS simultaneously. The depth control in network mode is set to steps of 10 m, which is adequate for engineering purposes. Should additional depth control be required, correlating our event discrimination schemes with a precise monitoring of groundwater level will allow for the precise depth location of events generated either at the fluid interface or above it.

Associating the weak impact events with M_L is selected here since it relates the observed energies to intuitively known scales. However, extending the standard distance correction curve (Richter 1958) must be explicitly stated to report M_L for events with distance below 10 km. Fig. 5, bottom part, summarizes the approaches by Bakun & Joyner (1984), Bullen & Bolt (1985), Di Grazia *et al.* (2001), Lahr (1989) and Richter (1958), whereby the solid part of each curve is the valid distance range given by the authors, the dashed part extrapolates to smaller distances with constant slope. Slope variation may result in more than a magnitude difference. M_L by HypoLine can adapt the slope according to actual attenuation profiles. Fig. 5, top inlet, shows the sinkhole monitoring at the Dead Sea: one single event is recorded by three SNS deployed at increasing distances: 30, 100 and 300 m. A slope of -1.0 for $-\log(A0)$ will adjust all measurements along one line, to $M_L - 1.4$ (more details below). This slope is in agreement with Bakun & Joyner (1984) but offset by -0.5 magnitude to approximate Lahr (1989) above 3 km.

CALIBRATION EXPERIMENTS

The monitoring of cavitation generated events at the Dead Sea offered a unique environment in which natural source processes can be simulated in the field at true scale, under controlled conditions and with minimal logistical constraints. This exclusive situation was exploited to link specific natural processes to signals, to verify the stability of the initial classification by sonogram analysis and to isolate the contributions of source process and transfer function to the final signal. The ultimate aim of the signal characterization conducted here is to enhance data processing, mainly optimizing the performance of pattern recognition and discrimination schemes.

Two types of material failures are expected to take place during cavitation: An initial failure takes place at the roof of the cavity, loosening material which then impacts a solid or liquid interface. At the roof, rock mechanics predicts the development of a plain tensile horizontal crack that propagates in mode-I (Scholtz 2002) within the layered medium, triggering an immediate stress release and causing inter-layer vibrations (Jaeger 1969). However, field simulations have shown that such events do not produce enough seismic energy for our sensors (0.1–75 Hz) to be detected at reasonable field monitoring distances (see below). In contrast, most of the sinkhole signals detected were generated by material impact either at the bottom of the cavity or at the brine interface.

Several types of impacts and material failures were simulated in natural sinkholes that were accessible (Figs 6 and 7). Experiments were all designed with one sensor nearest to the edge of the sinkhole where the experiment was taking place and lines of geophones with source-to-sensor distances ranging from 30 to 250 m. Source analogues consisted either of individual blocs of varying mass (5–30 kg) or of scree material, which was detached and pushed off the edge of sinkholes. Two impact scenarios were tested both in dry and brine-filled sinkholes: direct impact against the bottom of the sinkhole, or avalanche-like collapse processes within the trough of the sinkhole. The total fall height ranged between 5 and 14 m. In Fig. 6, the single bloc impacting against a bare rock interface (right) produced one broad-band spike, and the avalanche-like material collapse caused

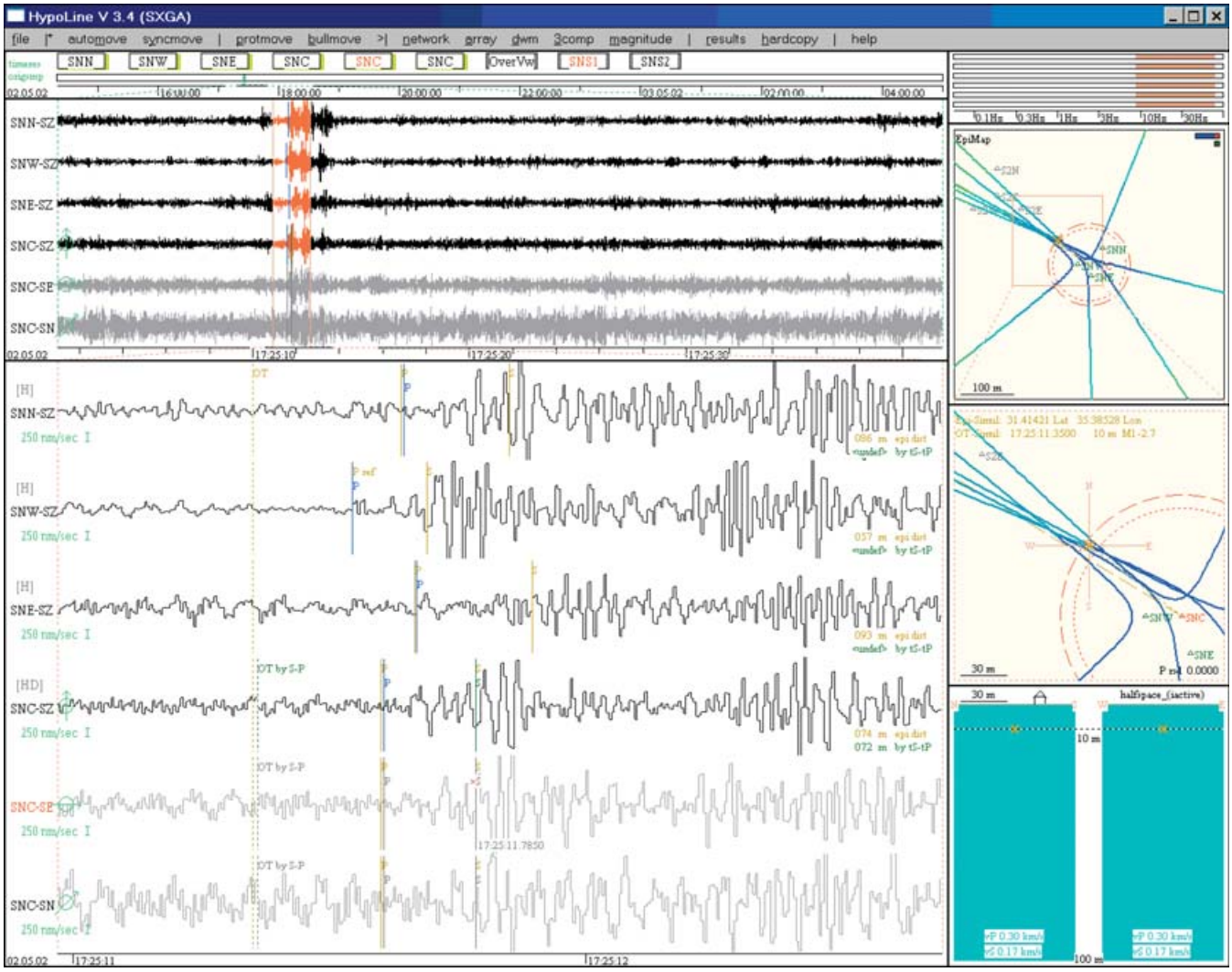

Figure 4. Screen dump of HypoLine, processing data of one SNS, that is, three 1-C and one centre 3-C seismograms in overview (40 s) and zoom (2 s) window. The right column windows display filter limits (9–80 Hz), epicentre map in overview (500*500 m^2) and zoom (150*150 m^2), and depth profile (0–100 m) of layer model (homogeneous half-space, v_P 300 m s^{-1}, v_S 170 m s^{-1}). The M_L −2.7 event (yellow X) is located 74 m NW the centre station (SNC, in red), that is, outside SNS aperture. Location constraints by hyperbolae and circles are marked in epicentre map; depth control (10 m) is displayed in layer stack. Time residuals between picked (blue, green) and simulated (yellow) phases are minor.

a lasting, emergent high-frequency signal. One individual bloc that impacted in brine-filled sinkhole (Fig. 7, right) triggered a rather impulsive lower-frequency signal. The complex-impact simulation (left) consisted of a single bloc followed by an avalanche-like material collapse, resulting in a lower-frequency signal with a rather impulsive onset followed by an extended coda. No cavity completely filled by fluid was accessible for simulations. In order to verify that the seismic signals recorded in the field are indisputably related to cavitation and sinkhole development, SNS were also deployed in areas along the Dead Sea shores where sinkholes cannot develop under the present conditions: the subsurface lithology is similar to that of the NH site but no salt layer is present and the groundwater level is much deeper (>50 m). Despite numerous noise bursts, no signal was detected which vaguely resembled standard sonogram patterns produced by sinkhole activity.

On the basis of these field simulations, the event types of Fig. 3 could be identified, and related to source processes. The first subgroup, #1 and #2, includes events that are rarely recorded. They are spike-like signals that have generally been detected by one single sensor. The signal #1 represents a final downwards displacement of some mm since the seismometer was placed on top of a dropping roof layer. This type of signal features very large local amplitudes. The signal #2 was generated by the simulation of tensile failure that is expected to take place at the roof of the cavity. Such failures were simulated both in nature and in a laboratory setting, and recorded by our instruments at extremely small source-to-sensor distances (10–50 cm), whereby different natural samples were gradually loaded till failure. The initial part of the signal, which records very weak episodes of brittle failure, is characterized by a series of very high-frequency spikes which are immediately followed by high-amplitude, low-frequency, damping-like signals produced by the destruction of the sample under non-confined conditions. Field tests also confirmed that the energy of these signals, in the 0.1–75 Hz window, is not detectable beyond source-to-sensor distance of a couple of metres under existing SNR.

The second subgroup comprises high-frequency events, #3 and 4. Their frequency range is broad (1–75 Hz) with a marked concentration of high frequencies (>40 Hz). Sonogram #3 has a short

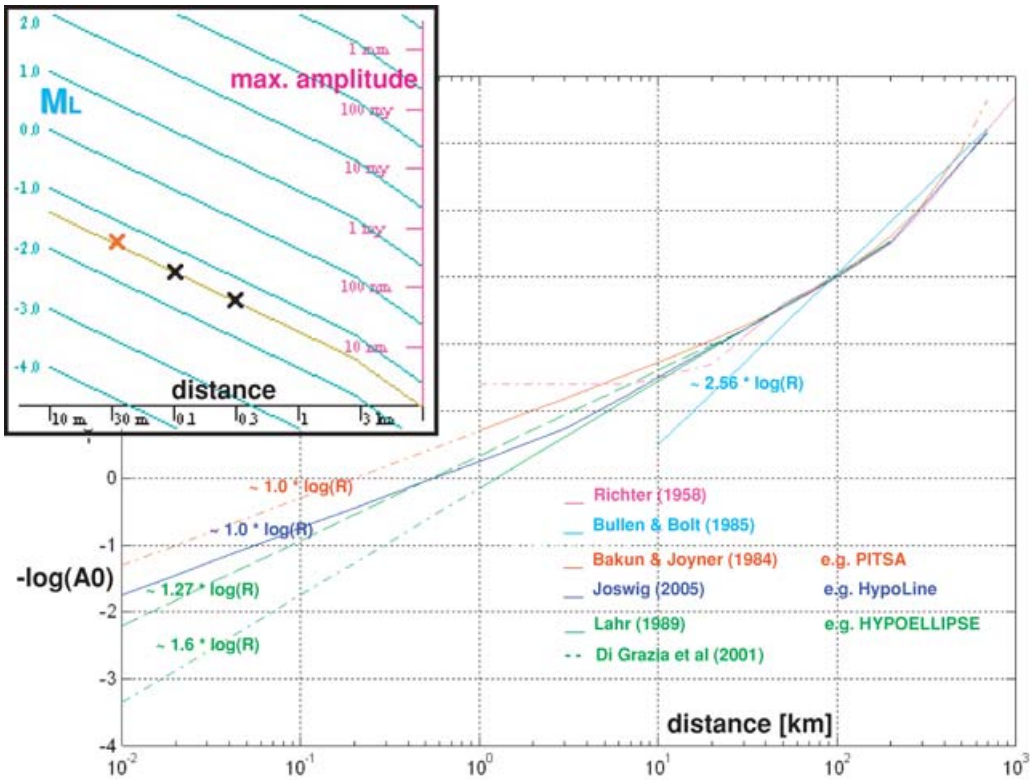

Figure 5. *Bottom:* Extrapolation of M_L distance correction factor $-\log(A0)$ for short slant distance R by different authors. The solid part of each curve is the valid distance range, while the dashed part is an extrapolation to smaller distances with original slope. *Top:* Calibration of magnitude–distance relationship. Wood-Anderson amplitudes of single event are plotted for distances of 30, 100 and 300 m. The slope of the relationship must match all data to define a common magnitude, here M_L −1.4 with slope −1.0.

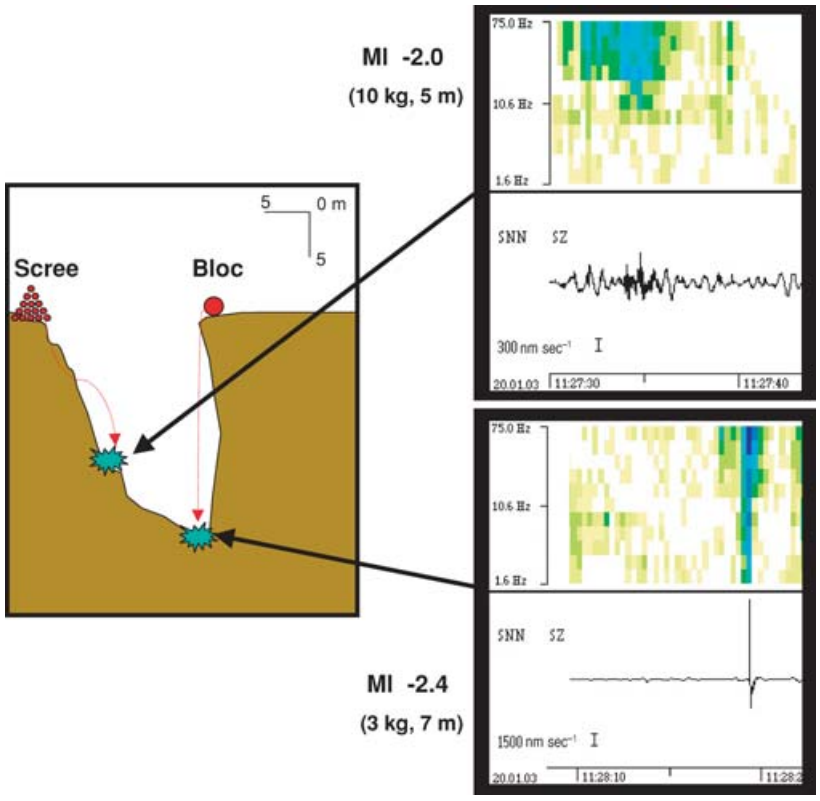

Figure 6. Source signal simulation in the field: Waveforms and sonograms generated by impacts in an open dry sinkhole by a rock-debris fall (top) and by a single bloc (bottom).

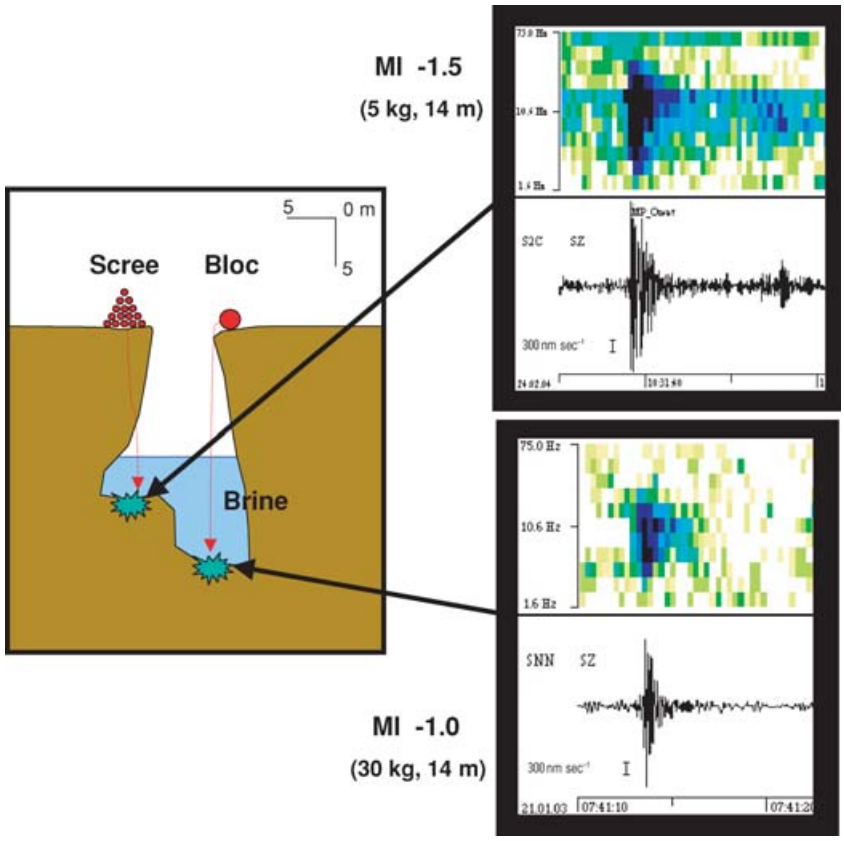

Figure 7. Source signal simulation in the field: Waveforms and sonograms generated by impacts in an open brine-filled sinkhole by a rock-debris fall (top) and by a single bloc (bottom).

duration (1–3 s), a very impulsive onset and a short coda. Sonogram #4 has a medium to long duration (5–20 s), an emergent onset and a long, extended coda. The signal envelope tends to be cigar-shaped with either a single lasting event or a series of pulses. Every single simulation of impacts on dry material produced a high-frequency signal that also belongs to this subgroup.

The third subgroup consists of low-frequency events, #5 and 6. These sonograms are characterized by the absence of high frequencies, above 40 Hz. The signal energy is concentrated between the middle and lower part of the spectrum (2–40 Hz), occasionally becoming almost monochromatic towards 6–10 Hz. Low-frequency tails are a dominant feature of these signals. Sonogram #5 corresponds to signals that have a short to medium duration (1 to 5 sec), a rather impulsive onset and a short coda. Sonogram #6 has an emergent onset and a long, extended coda. Its duration ranges between 5 and 30 s. Again, the signal envelope is cigar-shaped with either a single lasting event or a series of pulses. Some of these signals are reminiscent of low-frequency events produced by active volcanic systems (Chouet 1988, 1992, 1996; Wassermann 2002). Sonograms of this subgroup were recorded when simulating material impacts on the brine interface.

Although field simulations associated precise material failure processes with specific waveforms and sonogram types, the robustness of the analysis needs to be verified by characterization of source and propagation effects. It is necessary to exclude the possibility that a high-frequency signal generated by an impact on dry material would develop the characteristics of a low-frequency waveform typical of impacts at the brine interface by increased damping along its path. Additional field simulations were carried out to investigate the effect of bulk material attenuation and the effect of isotropic material attenuation. Investigations of the bulk material attenuation include: the scattering by numerous thin layers or mini-reflectors; the multipathing caused by lateral variation of layer thickness; and the anelastic behaviour of the unconsolidated material. The bulk material attenuation was tested systematically as a function of source-to-sensor distance for the type of source process that is most relevant to our investigations: impacts on dry material. Calibrated surface source processes (using a 5 kg hammer) were recorded at regular 20 m intervals along a series of 280-m-long lines, which stretched across zones where no geomorphologic evidence of sinkholes is visible. Fig. 8 compares standard waveforms (top) displayed in constant 3 s windows but varying amplitudes with their related sonograms (bottom), recorded at increasing source-to-sensor distances (from left to right; 20–280 m). The distribution of signal energy in the higher-frequency bands (40–75 Hz), which is critical for discriminating between impacts on dry material and impacts at the brine interface, remains stable throughout. In comparison, the seismograms (top) focus our perception on strong variations of signal amplitude and frequency.

Layered seismic velocity structures are used for standard event location by HypoLine. The log of borehole Hever-2 (Yechieli 2002) in Fig. 2 shows a dry unconsolidated media (0–23 m) underlain by a salt unit as well as a stable groundwater level, which is very near the material interface. Seismic velocities were calibrated at numerous locations with different layouts and spreads, taking into consideration sinkhole distribution and geomorphologic features. When measured in the vicinity (5–20 m) of visible clusters of sinkholes, *P*-velocities range between 260–380 m s^{-1}. These are unusually

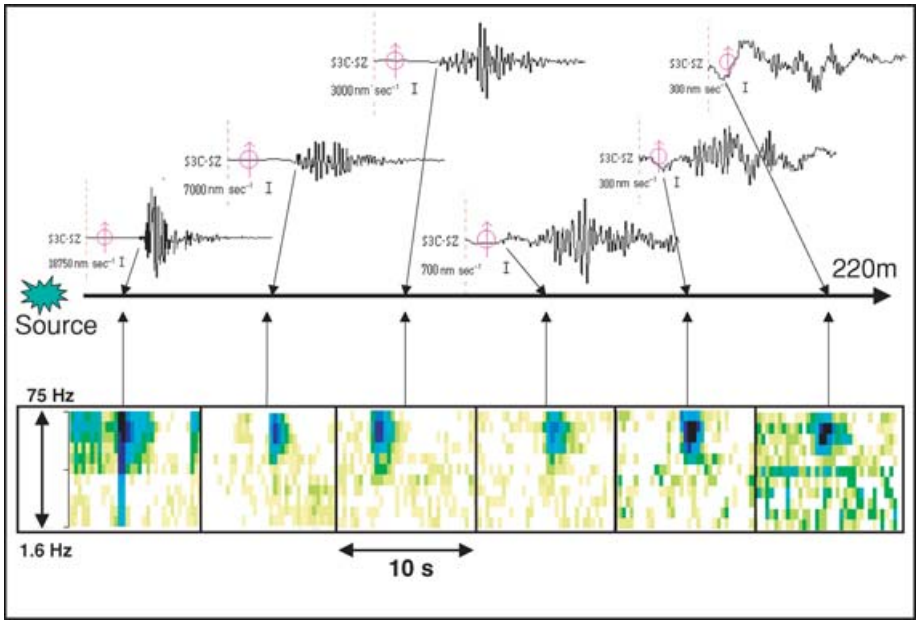

Figure 8. Stability of the sonogram analysis for source-to-sensor distances from 20 to 220 m. Sonograms display the vertical component in constant 10 s time windows. Corresponding waveforms with varying amplitudes (see scale bars) and constant 3 s window are displayed for comparison. The signal source is an impact at the surface.

low *Vp* values, departing significantly from 1100 m s^{-1} given by Shtivelman (1999) for the direct subsurface media in the same area (line RP-003). The discrepancy is related to a scaling issue. As the section studded by sinkholes represents only a small section (10–15 per cent) of the entire seismic lines (450–500 m) shot by Shtivelman (1999), velocities of over 1100 m s^{-1} represent an average for the near surface media over hundreds of metres. When measured at a scale of dozens of metres and within media that display a low degree of consolidation as well as a high concentration of discontinuities and voids, *Vp* values are significantly lower. Although very low seismic velocities are not common, beach sand has been reported to have velocities inferior to 230 m s^{-1} at shallow depth (0–25 m) (Bachrach *et al.* 2000). In our case of sinkhole investigations, a half-space model with a constant velocity of 300 m s^{-1} was used. This design is justified for short source-to-sensor distances (up to about 100–150 m) because it averages the velocities of a multitude of decimetre-thick layers that are too small to be properly resolved. At larger source-to-sensor distances, beyond the salt crossover, a simple two-layer model was designed on the basis of borehole information (Fig. 2). The top layer, consisting of dry unconsolidated material, has *Vp* of 300 m s^{-1}. The lower layer has *Vp* of 1800 m s^{-1}, which is the average velocity for the "salt layer" measured by Shtivelman (1999) in the NH area. Locating events with seismic velocities that significantly depart from those measured in the field (average 300 m s^{-1}) gave unreasonable solutions: sinkhole events were located deeper than the bottom of the salt horizon that can be reliably constrained by boreholes. The relocation of events that we simulated in the field (depth: 0–20 m) was also best validated by these two seismic velocity models. To relate determined M_L to our data, a series of projectiles (limestone boulders, concrete blocs, salt blocs and fossilized wood) were weighed (2 to 30 kg) and then thrown under controlled conditions into a brine-filled sinkhole whose level was located 14 m below surface. All simulations were recorded simultaneously by three SNS deployed at 30, 100 and 300 m from the source. The slope of the M_L to distance decay below 3 km was adjusted to fit these data. In the case of Fig. 7, a mass of 30 kg falling 14 m into the brine produces a M_L −1.0 event; a smaller mass of 5 kg causes M_L −1.5. A mass of 10 kg landing on scree material on the side of the sinkhole trough (Fig. 6) after a free fall of 5 m causes M_L −2.0, and a 3 kg mass impacting at the bottom of a sinkhole trough after 7 m free fall equals M_L −2.4.

MONITORING RESULTS

Since the calibration experiments validated the relationship between source processes and seismic signals recorded at the surface, SNS were deployed to monitor sinkhole activity. Fig. 9 displays the spatial distribution of four distinct sets of sinkhole events, which were monitored within the same sinkhole site NH within 12 hr periods, at night-time. The SNS (black circles) were repeatedly deployed at the same reference location (SNS centre: 0;0) for three surveys (2002 February, 2002 May and 2003 May). Because of flooding hazard, the SNS that recorded the 2003 January data set was deployed 200 m to the east and 100 to the north (SNS centre: −200;100). Events could well be detected within a radius of 150–200 m. The spatial distribution of the four sets is loosely spread within a large NW–SE trending cluster, located to the NW of the reference SNS. Each data set, however, shows different clustering patterns and source-to-sensor distances. Both 2002 February and 2002 May data sets display a cluster of events centred close to the SNS as well as many distant individual events. The 2003 January and 2003 May data sets show denser clusters of events, which are not centred on the SNS. Station relocation and data sparseness does not permit a detailed quantification of events distribution. However, it can be reasonably assumed that the apparent randomness of impact distribution that was repeatedly observed, within periods of several hours, indicates that the material that fails is of irregular size and quality. Since these events do not concentrate along specific features or within limited locations, it would suggest that subsurface material failures affect large areas and that cavitation systems are complex. Although the overall spatial distribution of events along a broad NW–SE trending band is partly biased by monitoring conditions, it

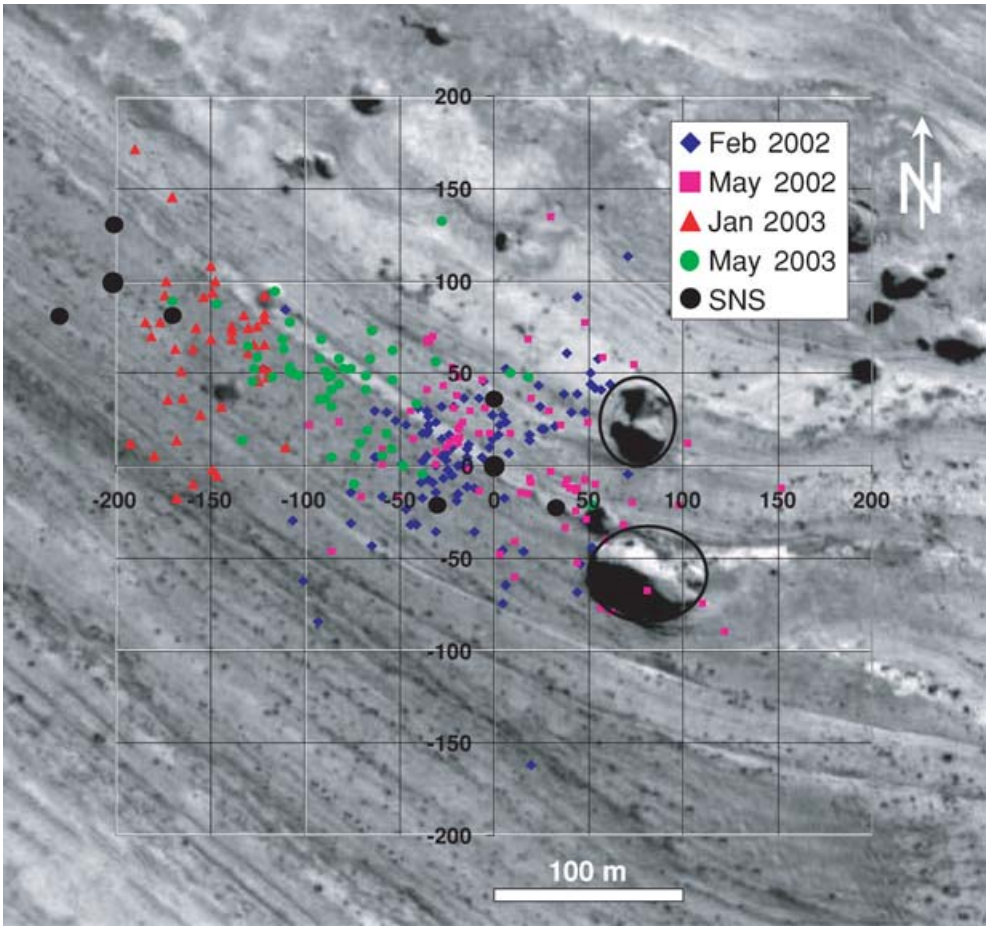

Figure 9. Location plot of sinkhole-generated events recorded at Nachal Hever site (Dead Sea) during four 12 hr periods. An air photograph (1999.02.12) of the same location with two fully developed sinkholes (black circles) is provided for comparative purpose. Black circles indicate the location of SNS and its sensors.

is in agreement with the direction of fault zones and lineaments of tectonic origin along the western Dead Sea Shores (Abelson *et al.* 2003). It can also be seen that most of the sinkhole events cluster to the N–W of two large visible sinkholes (circled in black, to the right of SNS) and that the event clustering migrates towards the N–W with time (2002 February, 2002 May and 2003 May). The NW area with dense clusters of sinkhole events is located below areas that did not show geomorphologic features of sinkholes at the time of monitoring. Incidentally, this exact area is where a series of sinkholes have developed and surface failures reached the surface since the summer of 2003. Except for rare avalanche type of material collapse, events were not recorded within existing mature sinkholes (circled in black, to the right of SNS). Although the data sets 2002 February and 2003 January were acquired during heavy rainfall, the number of sinkhole events detected does not depart significantly from those recorded during fair weather. It is indeed unlikely that rainfall would have an immediate effect on subsurface failures since the confining strength is not modified instantaneously by pore water (brine) pressure changes even though the porosity of the host media is high. Additional events could be caused by surface runoff, which might increase the amount of material being detached from the edges of mature sinkholes.

Fig. 10 shows the spatial distribution of sinkhole event energy. M_L range over two orders of magnitude ($-1.5 > M_L > -3.0$), whereby events with magnitudes between -2.0 and -3.0 clearly dominate. According to source energy calibrations previously discussed, such magnitudes correspond approximately to the impact of masses of several kilograms after a freefall of about 5 m. Event magnitudes are randomly distributed for source-to-sensor distances of up to 150–200 m. Beyond that distance and up to 350 m, attenuation dominates increasingly: only events with stronger source magnitudes ($M_L > -2.0$), are detected. The spatial distribution of magnitudes (Fig. 10) also displays a random pattern with a few loose clusters. This suggests that dominating heterogeneities within the media result in material failures that are unpredictable both in energy content and in location. Nevertheless, sinkhole events with larger energy contents are systematically concentrated in areas where failure is not yet visible from the surface. This would indicate that event magnitude could be associated with the maturity of sinkhole development: once cavitation has reached the surface, failure becomes limited to minor strain accommodation whose source energy is much reduced.

A more conclusive relation between signal characteristics and maturity of sinkhole development was found by the distribution of predominant types of impact source processes. Monitoring shows that impacts on dry material generally outnumber impacts at the brine interface by a ratio of 60 to 85 per cent. However, an inverse relationship of two low-frequency signals to one high-frequency signal was recorded on 2003 January. Although the spatial distribution of the two main subgroups of sinkhole signals seem to be initially

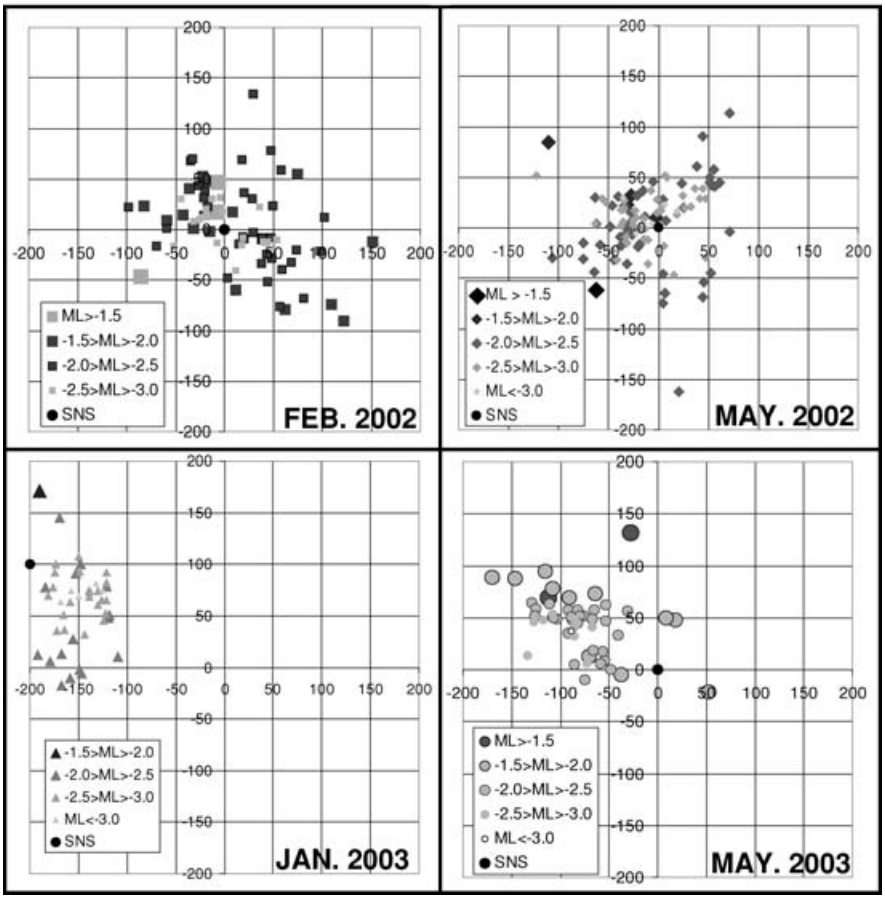

Figure 10. Spatial distribution and magnitudes for sinkhole events recorded at Nachal Hever site (Dead Sea) during four 12 hr periods. Symbol size is proportional to seismic event magnitude.

rather ubiquitous (Fig. 11), a high number of impacts at the brine interface cluster to the north–northwest (within the yellow circle) and the majority of high-frequency events are concentrated near the SNS and N–W of it (within the turquoise circle). It is worth noting that neither of the two areas displayed geomorphologic features directly related to cavitation until the last monitoring campaign (2003 May). Assuming that the groundwater table is stable throughout the NH site and limited to seasonal fluctuations of a few centimetres, the type of sinkhole events monitored is also indicative of impact depth and maturity of the cavitation process. Thus, sinkhole events monitored in the east (within the turquoise circle) are generated closer to the surface than those produced further to the west (within the yellow circle). This observation was confirmed both by the timing and the type of sinkholes that have developed soon after the spring of 2003: failure first reached the surface in the east and then extended westwards. Although monitoring was carried out either during rainfalls or during very dry periods, it does not appear to have favoured one specific type of sinkhole event over another. The high porosity of the material reduces fluctuations of the groundwater table to a minimum and limits the development of temporary perched water bodies. Monitoring the groundwater level regularly could be used, first, to verify standard source depth determinations and subsequently, to assess cavitation hazard by constraining the threshold between immature and mature (more hazardous) sinkhole development (Fig. 12).

The relationship between failing material masses and the magnitude of the seismic signals they generate may be further exploited to quantify geomorphologic changes and sinkhole development. An average of 200 sinkhole events of magnitude M_L −1.5 or less, are generated per 24 hr period. In the case of a typical underground fall height of 5 m, the mass of each material impact weighs about 20 kg, adding up to a total of maximum 4000 kg per 24 hr or 1500 tons yearly. A single sinkhole that opened north of the monitoring area over a period of a year was taken as a minimal reference for yearly volume change. With an average diameter of 17 m and depth of 11 m, it has a total volume of roughly 2500 m^3 and a material mass of approximately 5500 tons. Three factors contribute to explain the disparity between both approximations. First, the fall height of the material is quite variable. Thus, at the beginning of the cavitation process and whenever failure takes place at the edges of a mature cavity, the energy of the impact is too small to generate signal that can be detected. Second, since M_L computations are not duration based, it underestimates the energy of signals generated by extended avalanche-type material collapse. Third, large-scale material failures such as roof collapse (#1 of Fig. 3) are special events that are not easy to account for seismically. This rare type involves the failure of masses much larger than those associated with any single standard sinkhole event—just as the stress released by a single, big earthquake dominates that generated by a large number of aftershocks.

DISCUSSION

Seismic techniques were applied to monitor the dynamics of sinkhole development at an active site (NH) along the Dead Sea shore. A series of four data sets repeatedly recorded at the same location over a 15 month period was examined. Two specific types of

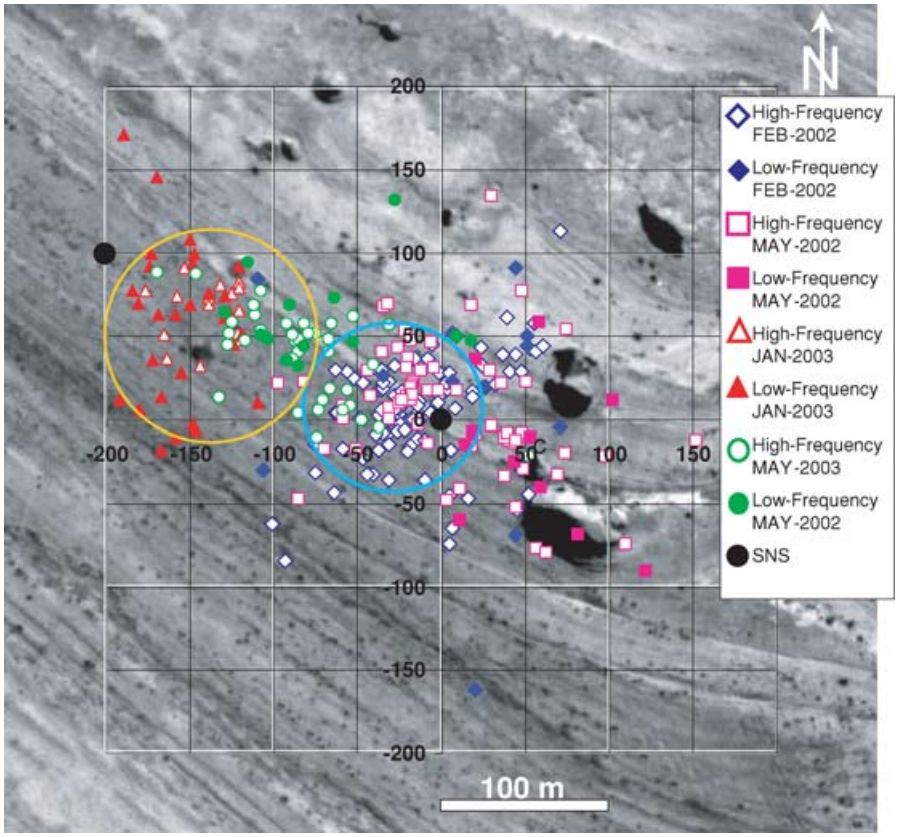

Figure 11. Spatial distribution of sinkhole event types recorded at Nachal Hever site (Dead Sea) during four 12 hr periods. Open symbols represent impacts on dry material. Impacts at the brine interface are indicated by filled symbols. The migration of nanoseismic events from the turquoise to the yellow circle denotes an evolution of the sinkhole activity.

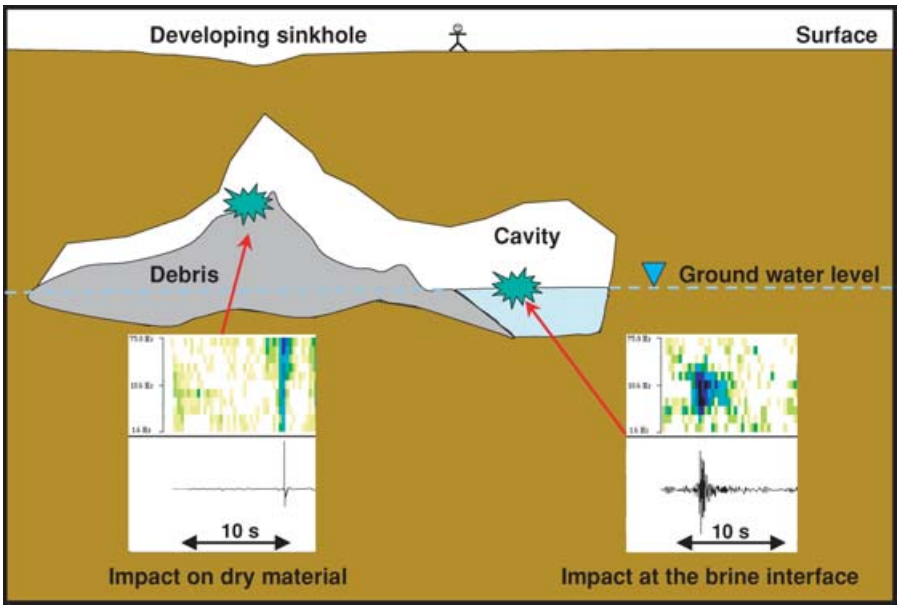

Figure 12. Schematic diagram of a sinkhole with two stages of cavitation maturity that are associated with impact type. The sonogram analysis allows the discrimination between dry impacts and impacts in brine-filled cavities, therefore, monitoring pre-collapse sinkhole activity.

impacts, (a) on dry material and (b) at the brine interface, both caused by cavitation-induced failure in sinkholes, were discriminated on basis of their sonogram signature. These processes take place at different depths, either at the ground water level or above it, and can be related to the maturity of the cavitation process. Numerous low-magnitude impacts on dry material were practically the only type of event recorded in zones where cavitation has reached the surface and where sinkholes are visible: they are the product of

final strain accommodation by mature sinkhole systems that have collapsed. In contrast, impacts at the brine interface of varying M_L were located in zones where cavitation has not yet reached the surface. Given an estimated groundwater depth of about 20 m at NH, low-frequency events of all magnitudes are indicative of cavitation at deeper levels and can be used to outline future sinkhole systems. The most worrisome type of sinkhole events are high-frequency signals of all magnitudes that were recorded below surfaces that presented no suspicious geomorphologic features: material failure is undoubtedly taking place above the 20 m groundwater depth. In fact, failure is most likely progressing within the top 10 m below the surface since the thickness of the salt layer that was originally dissolved reached 12 m.

It is worth noting that the presumption, based on nanoseismic monitoring, that cavitation was progressing towards the surface, to the west of existing sinkholes, was confirmed shortly after. Indeed, an extensive network of surface failures and visible sinkholes (located within the turquoise circle of Fig. 11) started developing during the summer of 2003. In terms of spatial distribution, recorded sinkhole events were dispersed over vast areas rather than concentrated within limited zones of sustained activity. This spatial dispersion of events was observed at two scales: within each of the continuous 12 hr monitoring sessions and over the 15 month intermittent monitoring period. This is a further indication that subsurface impacts are not confined to a single sinkhole or sinkhole cluster and this observation further supports the thesis of complex cavitation systems. In addition, it is expected that the extreme heterogeneity of the media would even enhance the inherent random pattern of cavitation taking place in unconsolidated composite material. This was confirmed by the detection of numerous mixed or imbricated seismic signals. Many cases of serial failures were recorded where several sinkhole events of different magnitude closely follow each other within a few seconds at a single location. It is now possible to map in detail the spatial distribution of subsurface failure as a function of time and to track cavitation dynamics before failure reaches the surface.

The scatter nature of the unconsolidated layered sediments in which cavitation is taking place is easily recognized when observing standard waveforms, which display strong material attenuation and scattering. However, our investigations show that sonogram analysis permits a reliable characterization of sinkhole generated signals and provides robust results. Nevertheless, it seems that the success of our investigations is also partly due to the fact that, despite unusually low seismic velocities ($\sim$300 m s^{-1}), resonance between the dominant wavelengths of sinkhole signals (10^2–10^0 m) and those of the natural layered media (10^0–10^{-3} m) was less important than originally anticipated. Even at their highest frequency range (75 Hz), the sinkhole signals we analysed, do not sample varves, laminae and centimetre-thin sedimentary layers and do not show particularly enhanced material attenuation. This also corroborates with the fact that $M_L - 3.0$ events can be detected at source-to-sensor distances exceeding 200 m. In terms of sinkhole event discrimination (impact on dry material vs. impact in liquid), it does not seem that the ubiquitous cut-off frequency (40 Hz), corresponding to a dominant wavelength of about 7.5 m, can be related to any systematic natural feature since the subsurface structures and cavities are known to have a totally random and irregular geometry. However, potential signal wavelength-structure interactions should be kept in mind while designing future field simulations under controlled conditions to investigate tectonics-waveform interaction.

CONCLUSIONS

Nanoseismic monitoring techniques were applied to extremely low-energy signals, generated by cavitation and sinkhole activity within an unfavourable SNR environment. Sonogram analysis was crucial for the success by (i) suppressing a multitude of noise bursts and (ii) discriminating between two basic subgroups (a) impacts on dry surfaces with high-frequency signals and (b) impacts in brines (low-frequency). The distinction works despite the strong, distance-dependent changes in the waveforms by scatter media. Conclusive information about the source processes underlying the two basic subgroups could be obtained by simulation experiments performed in the field at true scale and under controlled conditions. HypoLine was successfully used to locate individual sinkhole events by just a few, low-SNR seismograms, and an M_L scale, calibrated to very low magnitudes, estimated their source energy. Finally, the presence of high-frequency sonograms can be used to indicate that cavitation is taking place above the groundwater level and, therefore, progressing towards the surface.

ACKNOWLEDGMENTS

Dr Gideon Leonard, Israel Atomic Energy Commission (IAEC) initiated the application of nanoseismic monitoring to Dead Sea sinkholes; IAEC also funded part of this study. SNS equipment was by Minerva Dead Sea Research Center, Tel Aviv University (TAU) headed by Prof Ben-Avraham, who supported one of us (GHW-B). Dr Schattner (TAU) triggered numerous discussions and provided field support. Dr Yechieli and Dr Abelson (Geological Survey of Israel) introduced us to their sinkhole investigations. Dr Linda Bloch (TAU) edited the text, and Dr Marco (TAU) provided Fig. 1.

REFERENCES

Abelson, M., Kurzon, I., Crouvi, O., Wachs, D. & Yechieli, Y., 2002. Development Dead Sea sinkholes—detection from areal photographs up to 2001, *Geological Survey of Israel,* GSI/30/2002, 23 p.

Abelson, M., Baer, G., Shtivelman, V., Wachs, D., Raz, E., Crouvi, O., Kurzon, I. & Yechieli, Y., 2003. Collapse-sinkholes and radar interferometry reveal neotectonics concealed within the Dead Sea basin, *Geophy. Res. Lett.,* **30,** 1545–1549.

Arkin, Y. & Gilat, A., 1999. Dead Sea sinkholes: an ever-developing hazard, *Environmental Geology,* **39,** 711–722.

Bachrach, R., Dvorkin, J. & Nur, A., 2000. Seismic velocities and Poisson's ratio of shallow unconsolidated sands, *Geophysics,* **65,** 559–564.

Baer, G., Schattner, U., Wachs, D., Sandwell, D., Wdovinski, S. & Friedman, S., 2002. The lower place of the earth is subsiding—InSAR perspective, *GSA Bulletin,* **114,** 12–23.

Bakun, W.H. & Joyner, W.B., 1984. The M_L scale in Central California, *Bull. seism. Soc. Am.,* **74,** 1827–1843.

Bullen, K.E. & Bolt, B.A., 1985. *An introduction to the theory of seismology,* Cambridge Univ. Press, Cambridge, UK.

Butler, R., 2003. The Hawaii-2 observatory: observation of nanoearthquakes, *Seism. Res. Lett.,* **74,** 290–297.

Closson, D., Abou Karaki, N., Klinger, Y. & Hussein, M.J., 2005. Subsidence and sinkhole hazard assessment in the southern Dead Sea area, Jordan, *Pure appl. Geophys.,* **162,** 221–248.

Chouet, B., 1988. Resonance of a fluid-driven crack: radiation properties and implication for source of long-period events and harmonic tremor, *J. geophys., Res.,* **93B,** 4375–4400.

Chouet, B., 1992. A seismic model for the source of long-period events and harmonic tremor, in *IAVCEI Proceedings in Volcanology,* Vol. 3,

pp. 133–156, eds Jonson, R.W., Mahood, G. & Scarpa, R., Springer Verlag, Berlin, Germany.

Chouet, B., 1996. Long-period volcano seismicity: its source and use in eruption forcasting, *Nature,* **380,** 309–316.

Di Grazia, G., Langer, H., Ursino, A., Scarfi, L. & Gresta, S., 2001. On the estimate of earthquake magnitude at a local seismic network, *An. Geophys.,* **44,** 579–591.

Itamar, A. & Reizmann, Y., 2000. Air photo survey of sinkholes in the Dead Sea area. Geol. Survey of Israel, *Current Res.,* **12,** 21–24.

Jaeger, J.C., 1969. *Elasticity, fracture and flow,* Chapman and Hall, New York, 268 p.

Joswig, M., 1990. Pattern recognition for earthquake detection. *Bull. seism. Soc. Am.,* **80,** 170–186.

Joswig, M., 1995. Automated classification of local earthquake data in the BUG small array, *Geophys. J. Int.,* **120,** 262–286.

Joswig, M., 1999. Automated processing of seismographs by *Sparse Net, Seism. Res. Lett.,* **70,** 705–711.

Joswig, M., 2005. Second Stuttgart Summer School on Nanoseismic Monitoring, Course tutorial and SparseNet software, http://www.geophys.uni-stuttgart.de/sss05.html.

Joswig, M., Wust-Bloch, H. & Leonard, G., 2002. Nanoseismology: development of an integrated technique for the monitoring of nanoseismic events triggered by natural subsurface material failure, *Israel Atomic Energy Commission, Report #2791458,* 26 p.

Kafri, U., Goldman, M. & Lang, B., 1997. Detection of subsurface brine, fresh water bodies and the interface configuration in between by the TDEM method in the Dead Sea Rift, *Environmental Geology,* **31,** 42–49.

Lahr, J.C., 1989. Hypoellipse/version 2.0: a computer program for determining local earthquake hypocentral parameters, magnitude, and first motion patterns, *US. Geol. Surv. Open File Rep.* **89/116,** 81 p.

Lee, W.H.K. & Stewart, S.W., 1981. *Principles and Applications of Microearthquake Networks,* Academic Press, New York.

Nelson, R.G. & Haigh, J.H., 1990. Geophysical investigations of sinkholes in lateritic terrains, in *Geotechnical and environmental geophysics,* Vol. III, pp. 133–154, ed. Ward, S.H., Soc. Expl. Geophys., Tulsa.

Raz, E., 2000. Formation of sinkholes in the Dead Sea area—a surface survey, *Geological Survey of Israel, GSI/31/2000,* 52p.

Richter, C.F., 1958. *Elementary seismology,* Freeman, San Francisco, CA.

Rybakov, M., Goldshmidt, V. & Fleischer, L., 2000. Concealed sinkholes detection in the Dead Sea area using the microgravity technique—stage1; feasibility study, *Geophysical Institute of Israel, GII/841/93/99,* 14 p.

Schattner, U., 2003. Geodetic monitoring of surface deformation along the western shores of the Dead Sea using GPS and InSAR observations, *Geological Survey of Israel, Report, GSI/28/2003,* 71 p.

Scholtz, C.H., 2002. *The mechanics of earthquake and faulting,* 2nd edn, Cambridge University Press, Cambridge, UK, 471 p.

Shtivelman, V., 1999. Shallow seismic surveys in the sinkhole areas along the Dead Sea coast, *Geophysical Institute of Israel, GII/837/85/98,* 11 p.

Taqieddin, S., Abderahman, N. & Atallah, M., 2000. Sinkhole hazard along the eastern Dead Sea shoreline area, Jordan: a geological and geotechnical consideration, *Environmental Geology,* **39,** 1237–1253.

Wachs, D. *et al.*, 2000. Formation of sinkholes along the Dead Sea shore, *Geological Survey of Israel, GSI/41/2000,* 52 p.

Yechieli, Y., 2002. Borehole Hever 2: Geological and hydrological findings, *Geological Survey of Israel, GSI/8/2002,* 8 p.

Yechieli, Y. et al., 2004. Formation of sinkholes along the Dead Sea shore of the Dead Sea, *Geological Survey of Israel, GSI/21/2004,* 64 p.

Wassermann, J., 2002. Volcano Seismology, in *IASPEI New Manual of Seismological Observatory Practice,* Vol. 1, p. 42, ed. Bormann, P., GFZ Potsdam.

Wenjin, L. & Jiajian, X., 1990. Effectiveness of the high-precision gravity method in detecting sinkholes in Taian railway station of Shandong province, in *Geotechnical and environmental geophysics,* Vol. III, pp. 169–174, ed. Ward, S.H., Soc. Expl. Geophys., Tulsa.